Temperature Dependence of Entanglement and Coherence in Fenna-Matthews-Olson Complex

B González-Soria and F Delgado

Tecnologico de Monterrey, School of Engineering and Sciences, Mexico

E-mail: bgon@live.com.mx

Abstract. The high efficiency in excitation energy transfer observed in the Fenna-Matthews-Olson light-harvesting complex in green sulfur bacteria is due to its arrange of photo-pigments, called bacteriochlorophylls. They are central for the photosynthetic process of those bacteria being controversially associated to long-lived coherence. The study of this protein complex and its energy dynamics continues, trying to understand the environmental factors affecting it. This work explores the temperature effects in the behaviour of entanglement and coherence among bacteriochlorophyll excitation energy transfer within the Fenna-Matthews-Olson complex, considering the latest pigment-protein monomer arrangement of 8 bacteriochlorophylls. An analysis for the system evolution using the Hierarchical Equations of Motion method, a non-Markovian approach, is performed to get the global and semi-local entanglement, as well as the coherence in the system.

1. Introduction

The process of evolution has led some living organisms to develop highly efficient mechanisms to transform sun energy into biochemical energy using pigment-protein complexes in the photosynthetic process. Due to its water-soluble characteristics, the Fenna-Matthews-Olson (FMO) complex has been one of the most studied of these complexes for decades. It is a homotrimer, but a single monomer is shown in Figure 1a), depicting the 8 numbered bacteriochlorophylls (BChls) embedded in the protein scaffold. It shows the FMO structure with the eight inner BChls, their dipole momenta, and its scaffolding protein structure. Derived from the experimental spectroscopic studies, Figure 1b graphically shows the tracking of the energy transfer among BChls, signaling the three main entrance points coming from the baseplate: BChls 1, 6, and 8, with the main observed further interactions with the remaining BChls. Ultrafast spectroscopic studies reveal long time quantum coherence between the electronic states of the BChls [1], a mechanism of high transfer efficiency sampling the energy space through the excitonic superposition. The FMO complex of green sulphur bacteria has an energy transfer efficiency of a nearly 100% from the light-harvesting antennas (LHA) to the reaction center (RC) [2, 3]. Interest in studying the energy transfer dynamics within such an efficient system has brought together a diverse array of disciplines and theories in order to understand and to exploit quantum features in biology.

Proof of quantum coherence within the system has led to the application of quantum open systems (QOS) theory to study such phenomena in the quantum arena through the density matrix characterizing the energy statistical ensemble. The most common approaches: Redfield

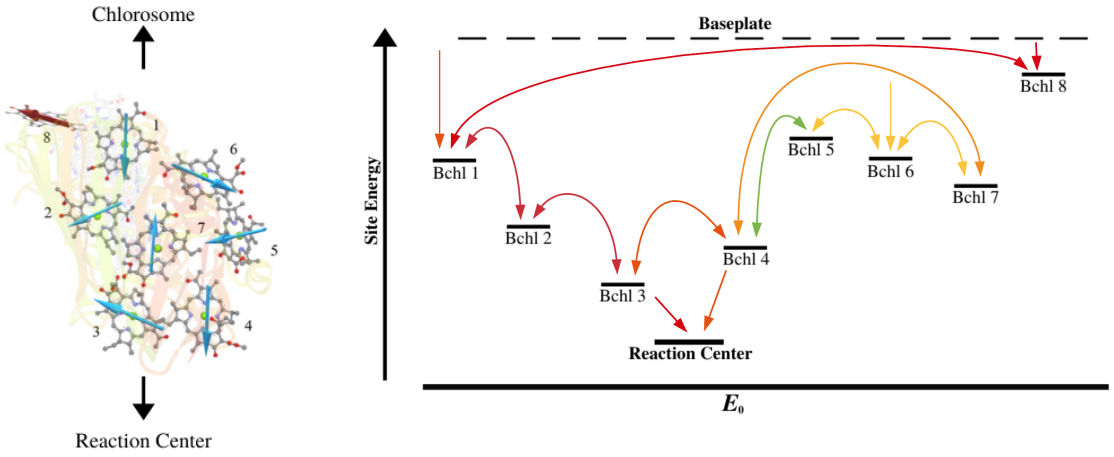

(a) **(b)**

Figure 1. (a) Single FMO monomer from *Prosthecochloris aestuarii* showing numbered BChls and corresponding dipole momenta. Figure produced from Protein Data Bank file 3EOJ. (b) Energy transfer diagram from higher energy BChls (1, 6, and 8), located closer to the baseplate, to the lower energy BChls (3 and 4).

and Lindblad master equations [4, 5], do not consider the non-markovian behaviour of the structure protein vibrations, modeled as a phonon bath interacting with the BChls. Alternative more realistic models should consider the bath relaxation, to understand the chromophore-protein interaction role on the energy transfer and the tuning effect on the site energies.

This work reproduces the excitation energy transfer among the eight BChls within each monomer of the FMO complex using the Hierarchical Equations of Motion (HEOM) method for the *Prosthecochloris aestuarii* green sulfur bacteria. We are centering our attention considering certain specific type of initial excitation in the initial stage. Second section discusses the statement of Hamiltonian for the system and the HEOM method [6] to solve the associated dynamical equations. Third section explains and discuses the raw outcomes obtained from a numerical simulation to then perform further analysis based on other physical quantities. Fourth section provides an analysis of entanglement and coherence achieved in the dynamics as the main goal of the article. Conclusions discusses an insight about the possible relation between the parametric effects on the population dynamics and the genetic traits of such complexes.

2. FMO complexes and their quantum dynamics simulation

Modelling of FMO complexes departs from a Hamiltonian H_S reproducing excitations due to electric dipole-dipole interactions among BChls (the *system*, S). Experimental analysis based on spectroscopy shows each BChl becomes excited in the first energy level and just one and only one at the time [7]. Then, the Hilbert space is just spanned by the excitation states obtained from the tensor product of $|0_i\rangle$ (ground state) and $|1_i\rangle$ (first excited state) for the entire system of N BChls ($N = 7, 8$ depending on the considered model): $|k\rangle \equiv |0_1 0_2 ... 1_k ... 0_N\rangle$, the *occupation* basis. While, the protein monomer where the BChls are embedded works as a scaffold. Since a protein has a large number of atoms compared to other molecules, vibrational states could be considered on the continuous regime: a phononic medium (the *bath*, B) exchanging energy with the set of BChls. It introduces a proper Hamiltonian H_B commonly described through proper basis depending on the dimension of such system. Finally, there are an interaction between both

systems depicted by H_{B-S}, which normally is modelled on a tensor product basis obtained from the natural basis for H_S and H_B. Here, we are barely explained each term of the Hamiltonian, but a more detailed reading is recommended, as instance [8]. The whole Hamiltonian and the density matrix ρ_T (S plus B) fulfils the von Neumann-Liouville equation:

$$H_T = H_S + H_{\text{reloc}} + H_B + H_{S-B} \quad \rightarrow \quad \dot{\rho}_T = -\frac{i}{\hbar}[H_T, \rho_T] \tag{1}$$

$$\text{with :} \quad H_S = \sum_{i=1}^{N} E_i |i\rangle\langle i| + \sum_{1\leq i,j\leq N} J_{ij}(|i\rangle\langle j| + |j\rangle\langle i|) \tag{2}$$

There, H_{reloc} is a term obtained by the displacement of the bath oscillators when they interact with th BChl's. Knowledge of E_i and J_{ij} are reported by [9, 10] for $N = 7, 8$ respectively, and they were obtained through spectroscopic experiments with several sulphur bacteria and some of their strains. In addition, the introduction of the bath B also moves the treatment into an quantum open system. Such systems should be modelled through extended canonical equations as Lindblad or Redfield master equations [11]. Those masters equations assume markovianity, which is applicable if the correlations between system S and environment B decay in a time scale that is much smaller than the evolution time of the entire system. It is not always the case for the FMO complex, so more sophisticated master equations should be considered.

Developed by [6] for phononic media and then applied to FMO by [12], HEOM method follows by switching into the interaction picture of H_{S-B} in order to trace the bath system considering non-markovian considerations. It becomes in recursive equations considering D previous temporal stages of the bath, each one labeled by a vector $\mathbf{n}$ of degree $s = 0, 1, ..., D$ (accounting the number of elements different of zero in the description) and by N for the BChl considered (see [8] for a more detailed explanation). There, $\rho_{\mathbf{n}}$ with $\mathbf{n} = (0, .., 0)$ is the approximation to the density matrix for the system and other $\rho_{\mathbf{n}}$ are auxiliary ones in each step of the recursive method, each one corresponding to all vectors $\mathbf{n} = (\mathrm{n}_1, \mathrm{n}_2, ..., \mathrm{n}_N)$ with $0 \leq \mathrm{n}_i \in \mathrm{Z}^+ \cup \{0\}$ such as $\sum_{i=1}^{N} \mathrm{n}_i = s$. It is a recursive procedure to better fit the evolution of the system under a non-markovian regime.

If k is the Boltzman constant, then $\beta = kT$. Subscripts $k \in \{1, 2, ..., N\}$ for each BChl should not be confused with the Boltzman constant in terms as $V_k = |k\rangle\langle k|$ and $\Delta_k = \lambda_k/\beta\hbar^2\gamma_k$ (λ_k is a reorganization term appearing in QOS due to the interaction with the bath). γ_i comprises the interaction strengths for H_{S-B} between the bath and each BChl coming from a bilinear model. HEOM model is written as:

$$\begin{aligned}\dot{\rho_{\mathbf{n}}} = & -\frac{i}{\hbar}[H_S + \sum_{k=1}^{N} \lambda_k V_k, \rho_{\mathbf{n}}] - \sum_{k=1}^{N} \mathrm{n}_k \gamma_k \rho_{\mathbf{n}} - r_{\text{trap}}(\{V_3, \rho_{\mathbf{n}}\} + \{V_4, \rho_{\mathbf{n}}\}) \\ & + i \sum_{k=1}^{N} \Delta_k([V_k, \rho_{\mathbf{n}_{k+}}] + \mathrm{n}_k([V_k, \rho_{\mathbf{n}_{k-}}] - i\frac{\beta\hbar\gamma_k}{2}\{V_k, \rho_{\mathbf{n}_{k-}}\}))\end{aligned} \tag{3}$$

See [8] for a more detailed description. BChls 1, 6 and 8, work as FMO antennas while BChls 3 and 4 drive the energy oscillations to the RC at the trapping rate, r_{trap}. If $\mathbf{n}$ is a vector of order s, then $\mathbf{n}_{k\pm}$ is the vector of order $s \pm 1$ obtained from $\mathbf{n}$ by increasing (decreasing) its component n_k by one. Last model has been considered for $N = 7$ to model the FMO complex dynamics [13]. Clearly, the treatment of the HEOM method is completely numerical. In addition, it is computationally convenient translate this equation into a superoperator-supervector version as it is detailed in [3, 8] dealing mainly with the model for $N = 7$. Despite $N = 7$ model was the first exploited by the research in the field, the eighth BChl was discovered as an important part

in the FMO complex functioning. Thus, for this work, next section solves numerically HEOM model for $N = 8$ case to simulate the dynamics, then analyzing the coherence and some global or bipartite entanglement measurements among FMO complex BChls.

Such set of differential equations requires a proper set of initial conditions. Several initial works in the field had considered localization states as initial conditions [3,5,13] as function of the spectroscopy studies [1, 9] which identifies the BChls first kicked by the energy flow, commonly BChls 1, 6, and 8 [5,10,13]. Despite easier, it is improbable that excitation begins with the exact excitation of only one entry BChl. Thus, another more feasible initial condition is referred as the Fluorescence Resonance Energy Transfer (FRET) or Förster resonance energy transfer [14]. Such initial condition gather an interaction and spread it on the most probable entries. Strictly, FRET initial condition is well-suited for research of protein interactions occurring between two molecules positioned within several nanometers of each other, as it occurs with the entry BCHls.

It is a mechanism which depicts the energy transfer between two light-sensitive molecules in the rate of the FMO complex global energies, then transferring such excitation to certain BChls as entries [15]. It is written as:

$$\rho^{i}_{\mathrm{FRET}} = \sum_{k=1}^{N} |\langle \epsilon_k | i \rangle|^2 |\epsilon_k\rangle\langle\epsilon_k| \tag{4}$$

where $\{|\epsilon_k\rangle | k = 1, ..., N\}$ are the eigenvectors of the Hamiltonian of the system, H_S. They are obtained numerically departing from the experimental Hamiltonian H_S.

3. Population dynamics in the FMO complex under a FRET initial condition

Thus, by solving the dynamics for one monomer of the FMO complex using the HEOM method for $N = 8$ BChls and $D = 3$, and sweeping uniformly different temperatures $T = 77, 131, 185, 239, 293$, and $347°K$, we trace the evolution of entanglement measures $\mathcal{C}_{\{kl\}}$, $\mathcal{C}_{\{k\}}$, and then the coherence $C_{l_1}(\rho)$ during the evolution in the interval time $0 - 15$ ps (such measures will be defined and discussed in the next section). Such range of temperatures were selected in the working window for the functioning of the FMO. While $77°K$ is the spectroscopic operation temperature where H_S was experimentally measured, $347°K$ is the higher temperature observed for live green sulfur bacteria.

We are using the FRET initial condition, ρ^{8}_{FRET}. There, the same characteristic parameters are used for all BChls: $\gamma_k = 50\mathrm{cm}^{-1}$, $r_{\mathrm{trap}} = 1\mathrm{ps}^{-1}$ and two reorganization energy values $\lambda_k = 35\mathrm{cm}^{-1}, 65\mathrm{cm}^{-1}$ [4] as comparison (as H_S, in the spectroscopic units, transformed to cm^{-1} dividing by $200\pi\hbar c$; cm^{-1} to s^{-1} with factor $200\pi c$). We are particularly using the reported Hamiltonian for the *Prosthecochloris aestuarii* bacteria [3].

Raw outcomes for the system populations are reported in the Figures 2 and 3 for $0-9$ps for a better appreciation (despite our simulations cover $0-15$ps, a sufficient time to observe the decay of coherence, which is computationally determined and extended for all simulations as a common simulation time), the more meaningful interval for the analysis before the coherence vanishes and excitation reaches their asymptotic equilibrium values. Thus, Figure 2 and 3 respectively exhibit the behavior for $\gamma_k = 50\mathrm{cm}^{-1}, \lambda_k = 35\mathrm{cm}^{-1}$ and $\gamma_k = 50\mathrm{cm}^{-1}, \lambda_k = 65\mathrm{cm}^{-1}$. Each BChl excitation behavior is represented in a different color in agreement with the color code included in figures a). In both cases, the initial excitation is located in BChls 8, 1, and 2 for the ρ^{8}_{FRET} initial condition. Despite, excitation in BChl 6 expected to be a main entrance, appears as a predominant secondary reaction. The increase of T implies generally a lower final excitation in BChl 3, the main output for the excitation as Figure 1b states. Note that the output through BChl 4 becomes limited for the current initial condition. A lower and faster excitation appears

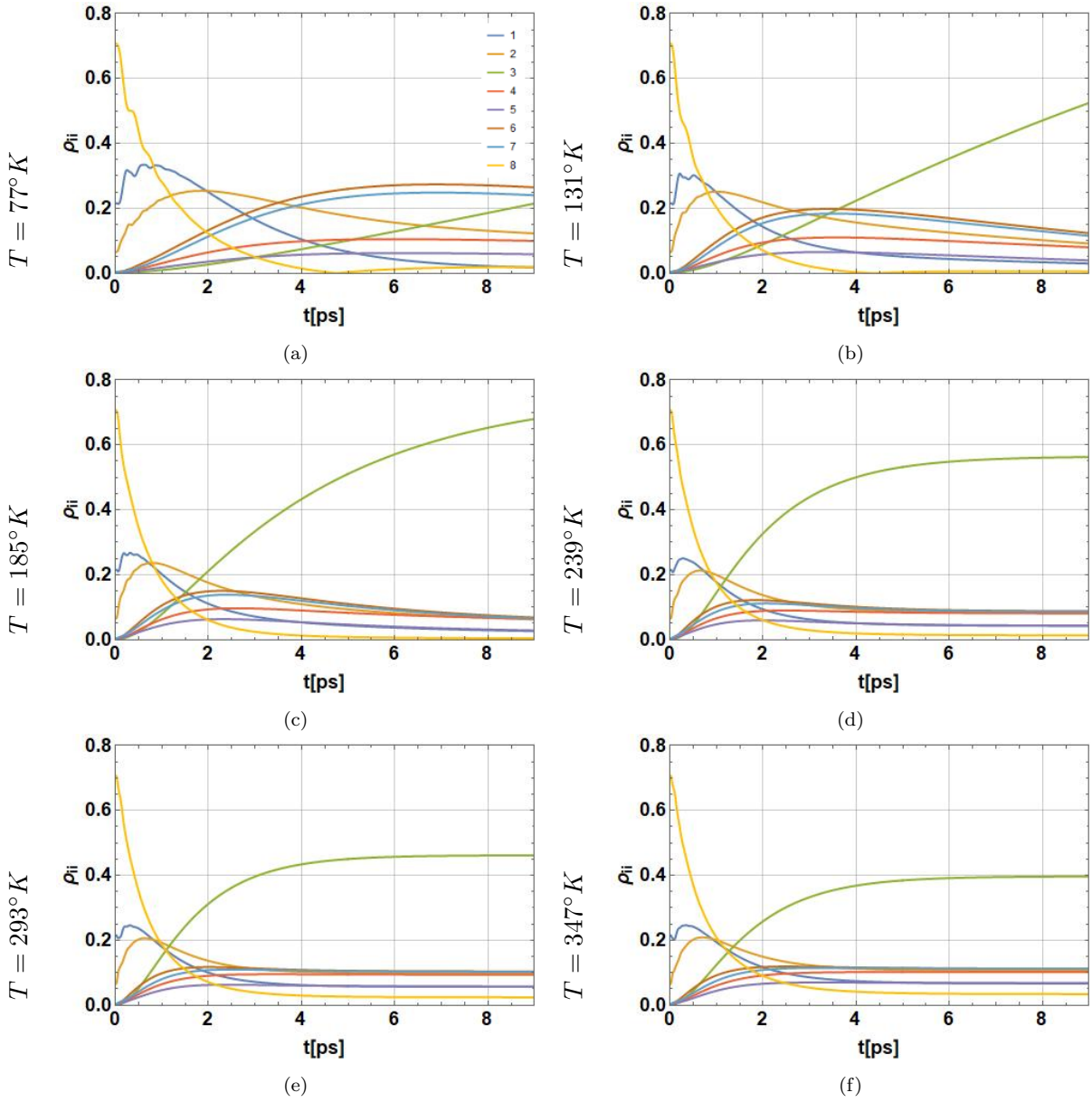

Figure 2. Population evolution of the FMO system during first 9ps of excitation energy transfer at temperatures (a) $77°K$, (b) $131°K$, (c) $185°K$, (d) $239°K$, (e) $293°K$, and (f) $347°K$ with the parameter $\lambda = 35\text{cm}^{-1}$. Parameter γ is set to a value of 50cm^{-1}. The common color legend is only included in the plot (a).

in general for $\lambda_k = 65\text{cm}^{-1}$. Thus, the equilibrium state is reached sooner in this last case, despite such effect reduces when T increases.

In the further analysis, the main interest is to study the entanglement relations among BChls through the coherence regime. Thus, in the following section, we will account for quantum derived properties derived from the dynamics for the coherence and entanglement in the process to compare them with previous outcomes for the model using $N = 7$ BChls and/or using occupation initial conditions.

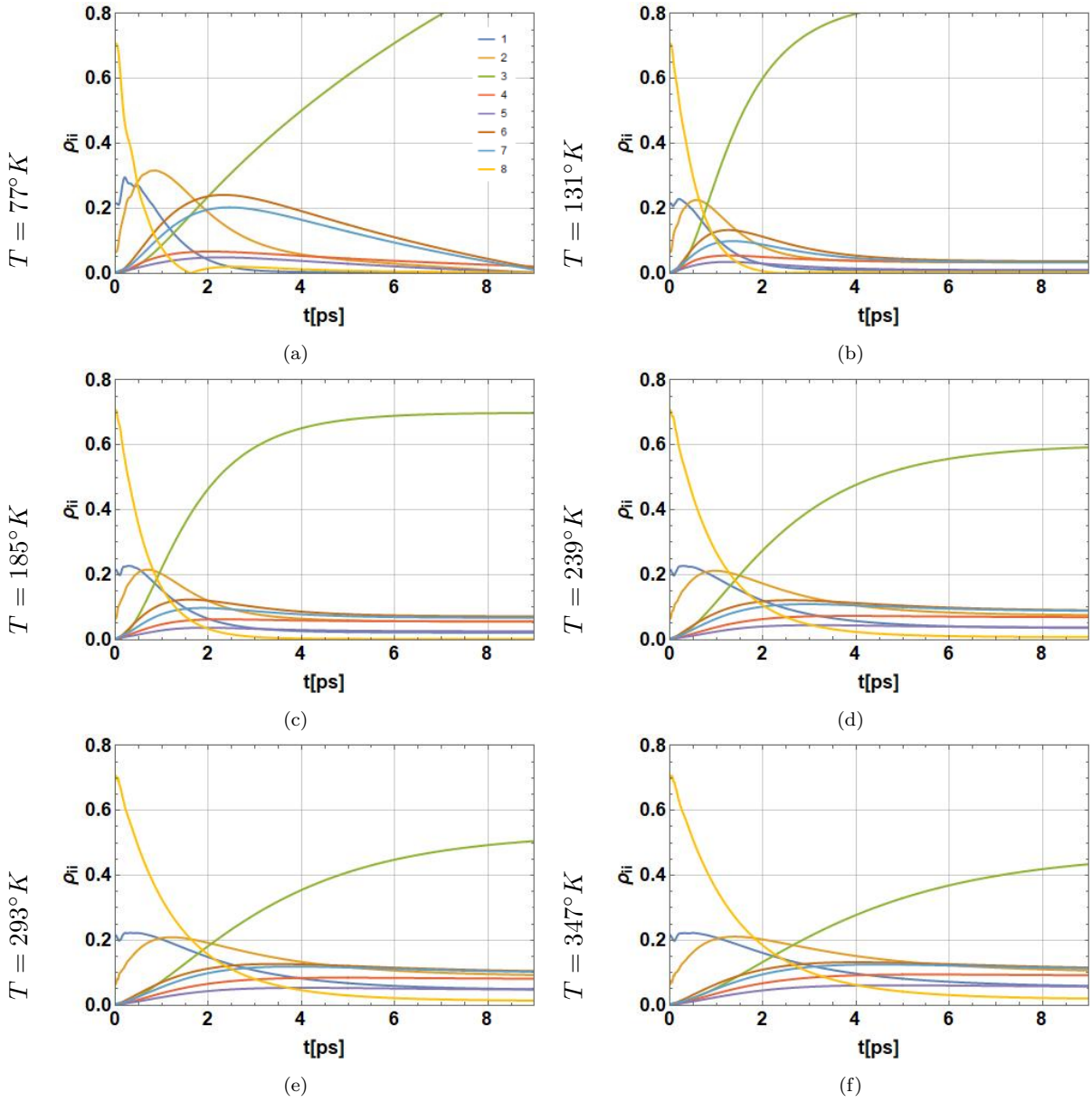

Figure 3. Population evolution of the FMO system during first 9ps of excitation energy transfer at temperatures (a) $77°K$, (b) $131°K$, (c) $185°K$, (d) $239°K$, (e) $293°K$, and (f) $347°K$ with the parameter $\lambda = 65\text{cm}^{-1}$. Parameter γ is set to a value of 50cm^{-1}. The common color legend is only included in the plot (a).

4. Entanglement in the FMO complex

In this work, we are interested in the analysis of entanglement for the model of $N = 8$ BChls. Together, we will analyze the associated coherence in the FMO. In fact, BChls exhibit an increase and holding of quantum coherence, in raw terms, the prevalence of terms $\rho_{ij}, i \neq j$ as the entries of ρ. A coherence measure based on the minimum distance from any non-coherent state:

$$C_{l_1}(\rho) = \min_{\sigma\in\Gamma} \sum_{ij} |\rho_{ij} - \sigma_{ij}| = 2\sum_{i<j} |\rho_{ij}| \in [0, d-1] \tag{5}$$

It is the l_1-norm [16]. Γ is the set of non-coherent states, with the minimum reached for $\sigma_{\rm diag} = \sum_i \rho_{ii}|i\rangle\langle i|$. The maximum bound is for $|\psi\rangle = \frac{1}{\sqrt{d}}\sum_{i=1}^{d}|i\rangle$. For the entanglement, we use the concurrences running from zero (separable) to one (maximally entangled), obtained by partially tracing ρ except for BChls k, l, $\rho_{kl} = {\rm Tr}_{\{kl\}}(\rho)$ or BChl k, $\rho_{\{k\}} = {\rm Tr}_{\{k\}}(\rho)$:

$$\mathcal{C}_{\{kl\}} \equiv \mathcal{C}(\rho_{\{kl\}}) = 2|\rho_{kl}| \in [0,1] \tag{6}$$

$$\mathcal{C}_{\{k\}} \equiv \mathcal{C}(\rho_{\{k\}}) = 2\sqrt{\rho_{kk}(1-\rho_{kk})} \in [0,1] \tag{7}$$

They are respectively interpreted as the entanglement a) among systems k, l [4], and b) between a system k and the remainder [3]. Both measures are obtained from the Partial Trace Criterion for bipartite entanglement. Note each pair entanglement contributes to C_{l_1} (5). All those measures are deeply discussed in [8].

We are fed the last formulas with the raw data for the BChls excitation obtained with the HEOM, thus obtaining time series for the evolution of the entanglement and the coherence. Figures 4a-b exhibits for $\lambda_k = 35{\rm cm}^{-1}$ and $\lambda_k = 65{\rm cm}^{-1}$ respectively, downwards, the entanglement measures $\mathcal{C}_{\{k\}}$ and $\mathcal{C}_{\{kl\}}$. The first measure is reported in the center of each figure and the second around it, employing the same type of plots used in [8]. In the plots, each one of the eight angular sectors around corresponds with each one of the BCHls (see the labels around: $k = 1, 2, ...8$). The central innermost sectors show the entanglement evolution of each BChl with the entire remaining system. Entanglement is reported in color in agreement with the color bar besides. Instead, external circular sectors report each BChl in relation with another BChl radially established (see the labels radially settled on the right: $l = 1, 2, ...8$). Each circular sector includes, in its two dimensional directions, the time evolution (counterclockwise, see the blue arrow with $t \in [0, 4]$ps) and the temperature (outwards, see the brown arrow with $T \in [77, 347]^\circ K$). With BChl 8 assumed initially excited through the $\rho(0) = \rho^8_{\rm FRET}$ condition, plots exhibit the strong sudden initial entanglement $\mathcal{C}_{\{k\}}$ between each BCHls $8, 1$, and 2 and the remaining system, which turns off before 1ps. While paired entanglement, $\mathcal{C}_{\{kl\}}$, becomes larger for low temperatures between $(2, 6)$, $(3, 4)$, $(4, 5)$, $(4, 7)$, $(5, 6)$, $(5, 7)$, $(6, 7)$, $(8, 1)$, and $(8, 2)$ pairs of BChls. Paired entanglement is particularly large between $(1, 2)$ pair in the initial time period. As well, a large and sustained entanglement appears for BChl 3 and the remaining system in the middle of the time evolution reported, which is larger for lower temperatures.

Comparing with the analysis performed using the initial condition $\rho(0) = |8\rangle\langle 8|$ [17], here, entanglement involving the BChl 2 appears as a difference, being sudden since the beginning instead delayed as there. In addition, a clearer relation of the pair entanglement is exhibited here with the previous description involving the cascade effect being presented in the Figures 4a-b. Because system states are depicted through localization states on BCHls, entanglement between BCHls localization states directly refers to the existence of paths through energy excitation is moving. First, an initial and fast entanglement appears between BCHls 8 and 1, then BChl 2 becomes suddenly involved. Thus, the last transfer excitation depicted moves to BChl 6. It then to the BChl 5 and 7. BChls 6 and 7 finally move such excitation to BChl 4 and finally this to BChl 3. The entanglement level is higher for lower temperatures and more long-lived for $\lambda_k = 65\,{\rm cm}^{-1}$.

Because coherence $C_{l_1}(\rho)$ is the sum of all concurrences $C_{\{kl\}}$, such quantity represents in average the presence and sustaining of paired entanglement. Figure 5a-b shows coherence $C_{l_1}(\rho)$

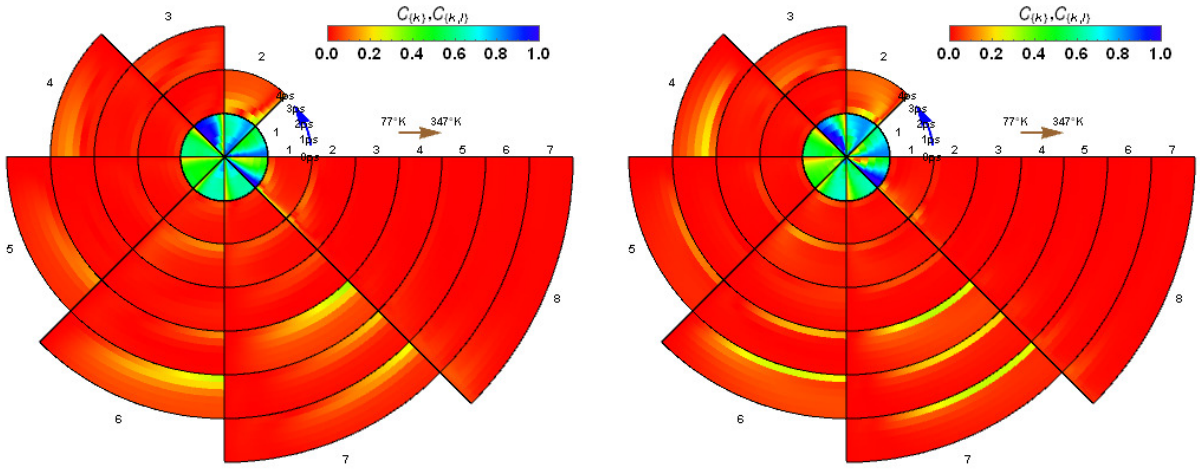

(a) **(b)**

Figure 4. Entanglement color chart for $\gamma_k = 50\,\mathrm{cm}^{-1}$ with (a) $\lambda_k = 35\,\mathrm{cm}^{-1}$, and (b) $\lambda_k = 65\,\mathrm{cm}^{-1}$. In the center, concurrence $\mathcal{C}_{\{k\}}$ evolution for each BChl, and in the outer tracks $\mathcal{C}_{\{kl\}}$ between different pairs in the crossing of each circular track and each angular sector. Time grows counterclockwise in $[0, 4]$ps on each angular sector. Temperature grows radially outwards on each track in $[77, 347]\,^\circ K$.

for $\lambda_k = 35\,\mathrm{cm}^{-1}$ and $\lambda_k = 65\,\mathrm{cm}^{-1}$ respectively. Color for each temperature is depicted in the common central code. As previously observed, fast and long-lived coherence is present for the larger λ_k. Together, the larger values of coherence are related with the lower temperatures. Interestingly, sudden initial peaks reported for $C_{l_1}(\rho)$ in [17] disappear using the $\rho(0) = \rho^8_{\mathrm{FRET}}$ condition instead $\rho(0) = |8\rangle\langle 8|$. Comparing both outcomes, we note that a large long-lived coherence is produced by such initial condition.

5. Conclusions

We have analyzed the evolution of quantum excitation of the Fenna-Matthews-Olson complex for *Prosthecochloris aestuarii* bacteria in the model including its eight BChls. By using the method to model the dynamic evolution of one monomer and sweeping a set of temperatures in the operation range, we tracked the boost of long-live coherences via localized entanglement using the FRET initial condition ρ^8_{FRET}. Such data evolution fed the measures $\mathcal{C}_{\{k\}}$ for single entanglement with the system and $\mathcal{C}_{\{kl\}}$ for entanglement by pairs of BChls. Coherence has been analyzed using the measure C_{l_1}.

A more detailed dynamics in the entanglement evolution has been found as compared with previous analysis involving eight BChls but the simpler occupation initial condition $\rho(0) = |8\rangle\langle 8|$ [17]. As well, a different profile for the evolution of the coherence was found, revealing a different behavior to that reported in [8,17]. Instead of a sudden peaked coherence for $\rho(0) = |8\rangle\langle 8|$ initial condition, a more long-lived sustenance has been found. The faster processes and larger values for those measures have been found for lower temperatures. In addition, larger reorganization energies boost the sustained entanglement between BChls 3 and 4, a faster establishment of entanglement in other pairs of BChls (but more limited for low temperatures). The same is barely true for coherence, despite such speed up also appear limiting the long-lived sustaining. Thus, reorganization energy λ_k values suggest an important role in the time scale and the

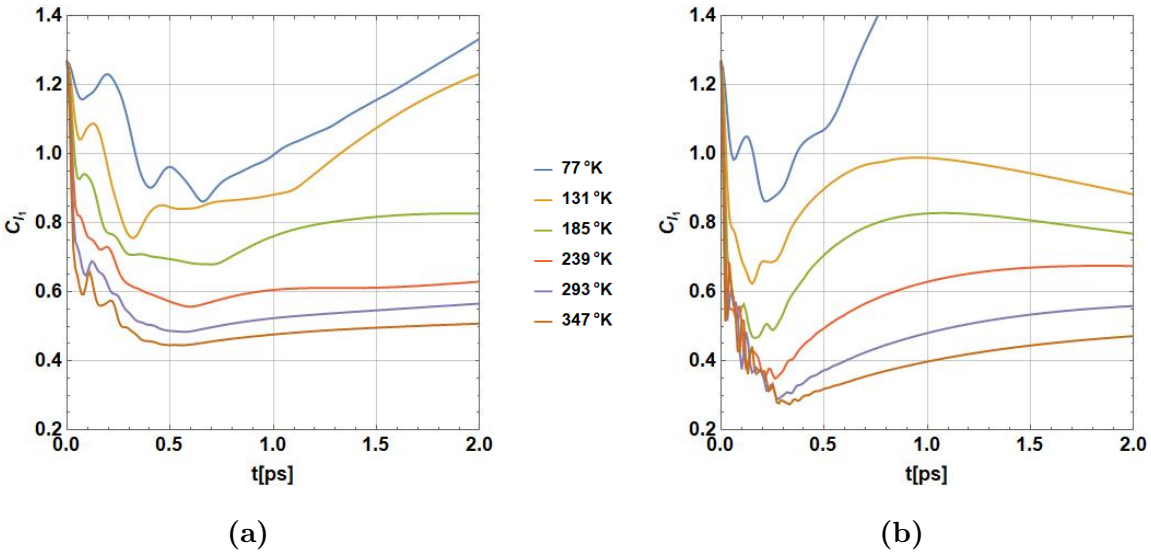

Figure 5. Coherence temperature dependence evaluated using norm-l_1, C_{l_1} for (a) $\lambda_k = 35\,\mathrm{cm}^{-1}$, and (b) $\lambda_k = 65\,\mathrm{cm}^{-1}$, during the first 2ps of evolution.

behavior of coherence. In fact, λ_k values set a damped behavior reducing the quantum coherence in the BChls, thus moving them into a statistical mixture of states, thus removing entanglement and coherence. Such values are not strictly known for each BChls, instead just representative values for the overall BCHls are considered in the literature [11]. Then, their knowledge becomes important to reach the precise time of long-lived coherence in the FMO. As a result, a nearer description of the theoretical models has been reached, particularly reflecting the spectroscopic characterization data.

An interesting feature analysed by [8] corresponds to variations found between species and strains (as instance for *Chlorobaculum tepidum* specie). Despite differences in the Hamiltonian, long-lived coherence and still efficiencies are completely similar. In addition, mutations have shown that those effects are still persistent.

Acknowledgements

The authors also like to acknowledge José Javier Rodríguez Mota for his support running the software required for generating the data used in this article.

References

[1] Engel G, Calhoun T, Read E, Ahn T, Mančal T, Cheng Y, Blankenship R, Fleming R 2007 *Nature* **446** 782
[2] Fenna R, Matthews B and Olson J 1978 *J. Mol. Biol.* **131** 259–285
[3] González-Soria B and Delgado F 2020 *J. Phys. Conf. Ser* **1540** 012026
[4] Sarovar M, Ishizaki A, Fleming G and Whaley K 2010 *Nat. Phys.* **6** 462-467
[5] Jesenko S and Žnidarič 2012 *New Journal of Physics* **14** 093017
[6] Tanimura Y and Kubo R 1989 *Journal of the Physical Society of Japan* **58** 101-114
[7] Weidemüller M 2009 *Nat. Phys.* **5** 91-92
[8] González-Soria B, Delgado F and Anaya-Morales A 2020 *Appl. Sci.* **10** 6474
[9] Adolphs J and Renger T 2006 *Biophysical Journal* **91** 2778–2797
[10] Schmidt M, Müh F, El-Amine M and Renger T 2011 *J. Phys. Chem. Lett.* **2** 93-98
[11] Palmieri B, Abramavicius D, Mukamel S 2009 *J. Chem. Phys.* **130** 204512
[12] Ishizaki A and Fleming G 2009 *J. Chem. Phys.* **130** 234111
[13] Kreisbeck C, Kramer T, Rodríguez M and Hein B 2011 *J. Chem. Theory Comput.* **7** 2166–2174
[14] Jang S, Newton M and Silbey R 2004 *Phys. Rev. Lett.* **92** 218301

[15] Leon-Montiel R, Kassal I, Torres J 2014 *Transport. J. Phys. Chem. B* **118** 10588
[16] Horn R and Johnson C 1991 *Matrix Analysis* (Cambridge University Press, Cambridge, England).
[17] González-Soria B, Delgado F and Anaya-Morales A 2021 *J. Phys. Conf. Ser* **1730** 012033